Chemical Engineering Journal 547 (2026) 180810

Contents lists available at ScienceDirect

Chemical Engineering Journal

journal homepage: www.elsevier.com/locate/cej

Kinetics of pure and industrial hematite powder reduction with hydrogen and carbon monoxide mixtures

Antonio D'Angelo [a,b,*], Emiliano Salucci [a,b], Vincenzo Russo [b], Martino Di Serio [b], Henrik Grénman [a], Henrik Saxén [a]

[a] Åbo Akademi University, Henrikinkatu 2, Åbo, FI-20500, Finland
[b] Università degli studi di Napoli Federico II, Via Cintia, Napoli, IT-80126, Italy

ARTICLE INFO

Keywords:
Iron oxide
Morphology
Gas solid reaction
Experimental investigation

ABSTRACT

The steel industry plays a key role in society and the global economy, but it also has a significant environmental impact. The fossil-based process utilizes blast furnaces, in which coke acts as a reducing agent and energy source, which is why it accounts for about two gigatons of CO_2 emissions on an annual basis. Reducing iron oxides with hydrogen instead of carbon monoxide provides an elegant carbon-free alternative with water as the byproduct. However, the rapid advancement of this technology on the market would require extremely large investments in entirely new reactors and reactor systems. Moreover, the current and foreseeable hydrogen capacity and infrastructure are insufficient to meet the demand, and the price of non-fossil hydrogen is still high. An alternative to reducing emissions would be to adapt current reactor infrastructure to flexibly utilize mixtures of carbon monoxide and hydrogen, depending on hydrogen availability and price. This dynamic approach requires a rigorous understanding of the reduction kinetics of iron oxides with varying gas composition and reaction conditions. The present work studies the kinetics of pure and industrial hematite powders using H_2 and CO mixtures in small scale in the laboratory. The reduction process was followed by analyzing the off-gases online, and the physical-chemical behavior of the solid phase during reduction was studied through detailed analysis of partially reduced material obtained at different stages of the reduction process. The experimental data revealed critical factors influencing the reduction of kinetics, both qualitatively and quantitatively, which support understanding of the complex overall process. Moreover, the study revealed significant differences between pure hematite and industrial feedstock.

1. Introduction

The scientific community has brought attention to the topic of climate change through its extensive discussion. Excessive CO_2 emissions into the atmosphere are the main cause of climate change. The iron- and steelmaking sector, satisfying the huge global demand of steel in the world of almost 2000 million tons annually, is a main contributor to global CO_2 emissions. A majority (~ 70%) of the production is ore-based using the blast furnaces (BF, Fig. 1.a), where the reductant is coal of fossil origin [1]. In this process, a partial combustion of the coke that is charged at the top together with iron oxide, forms carbon monoxide that gradually reduces the ore at high temperatures while ascending in the furnace [2,3,4]. The reaction pattern, summarized in eqs. 1.a - g, proceeds in several partly overlapping steps from hematite through magnetite and wüstite to metallic iron. Side reactions such as the reverse Boudouard reaction, the combustion of carbon monoxide, and partial gasification of carbon also play important roles for process.

$$3Fe_2O_3 + CO \rightleftarrows 2Fe_3O_4 + CO_2 \quad (1.a)$$

$$Fe_3O_4 + CO \rightleftarrows 3FeO + CO_2 \quad (1.b)$$

$$FeO + CO \rightleftarrows Fe + CO_2 \quad (1.c)$$

$$Fe_3O_4 + 4CO \rightleftarrows 3Fe + 4CO_2 \quad (1.d)$$

$$2C + O_2 \rightleftarrows 2CO \quad (1.e)$$

$$2CO + O_2 \rightleftarrows 2CO_2 \quad (1.f)$$

$$2CO \rightleftarrows C + CO_2 \quad (1.g)$$

* Corresponding author at: Åbo Akademi University, Henrikinkatu 2, Åbo, FI-20500, Finland.
E-mail address: antonio.dangelo@abo.fi (A. D'Angelo).

https://doi.org/10.1016/j.cej.2026.180810
Received 28 May 2026; Received in revised form 7 August 2026; Accepted 15 August 2026
Available online 19 August 2026

The reverse Boudouard reaction is defined as the disproportionation of CO into carbon dioxide and carbon. It is strongly temperature dependent, and the exothermic reaction occurs in a wide range of temperature between 400 °C and 1000 °C and can be catalyzed by various oxides [6,7,8]. The equilibrium dependence of the direct and reverse reaction between carbon monoxide and carbon dioxide is expressed in Fig. 2.

It displays the relative amount of the two species at equilibrium at different temperatures. For temperatures $T > 900$ K, equilibrium is shifted to form CO [9]. Vice versa, at low temperature, carbon deposits are favored. The entire reduction process displays a complex behavior between solid and reducing gas where also gangue components may play a role. Finally, molten iron with dissolved carbon, called hot metal, is taped out from the lower part of the blast furnace and is transferred to a basic oxygen furnace (BOF) to form crude steel. The principal alternative to classic BF route is the direct reduction (DR) processes in which reformed natural gas reduces iron ore in a shaft furnace by gas-solid reactions [10,11,12]. The combination of shaft furnace (Fig. 1.b) and electric arc furnace (EAF), which melts the iron and removes (some) gangue, offers several advantages such as a potential reduction of CO_2 emissions by up to 50% and lower energy cost due to the lower temperature applied, 800 °C < T < 1200 °C in the DR furnace. The temperature, the pressure and the H_2/CO ratio are important operative parameters and differ between the processes applied. The most common ones are the HYL-III (today termed Energiron) and the MIDREX processes [13,14]. The reduction steps by hydrogen are

$$3Fe_2O_3 + H_2 \rightleftarrows 2Fe_3O_4 + H_2O \quad (2.a)$$

$$Fe_3O_4 + 4H_2 \rightleftarrows 3Fe + 4H_2O \quad (2.b)$$

$$Fe_3O_4 + H_2 \rightleftarrows 3FeO + H_2O \quad (2.c)$$

$$FeO + H_2 \rightleftarrows Fe + H_2O \quad (2.d)$$

The simultaneous presence of hydrogen and carbon monoxide complicates the reaction pathway of pure hydrogen reduction [15,16]. The influence of the reverse Boudouard reaction on the process, combined with the thermodynamics of the reduction using CO and H_2 is depicted in Baur-Glässner plot (Fig. 3). It is an equilibrium diagram that

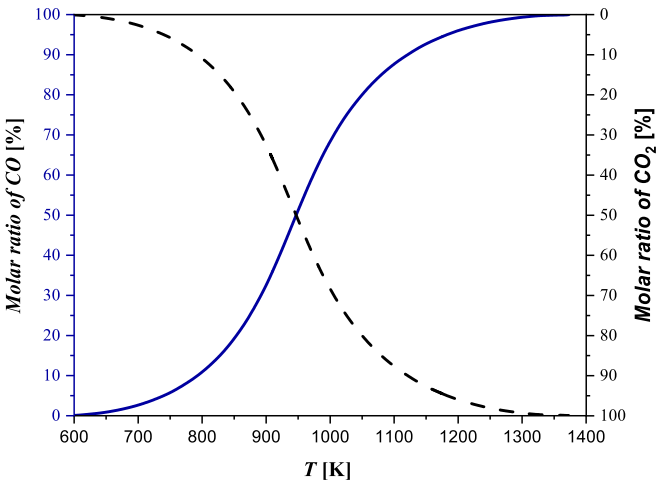

Fig. 2. Boudouard equilibrium diagram at atmospheric pressure calculated with Fact Sage 8.2 [5].

reports the Gas Oxidation Degree (*GOD*), defined as the molar ratio between the oxidizing species and the sum of the oxidizing and reducing species, as a function of the temperature.

$$GOD = H_2O/(H_2 + H_2O) \quad (3.a)$$

$$GOD = CO_2/(CO + CO_2) \quad (3.b)$$

GOD can be thought of as the complement of the driving force of the process, in which a lower *GOD* corresponds to a higher driving force and vice versa.

In addition, the water–gas shift (WGS) reaction (Eq. 4) influences the gas composition.

$$CO + H_2O \rightleftarrows CO_2 + H_2 \quad (4)$$

The shift in gas composition can have a significant influence on the reduction kinetics, as the CO:H_2 ratio changes [17,18,19,20,21]. As displayed in Fig. 4, the equilibrium of water gas shift reaction is displayed as function of the molar ratio of the species involved in the

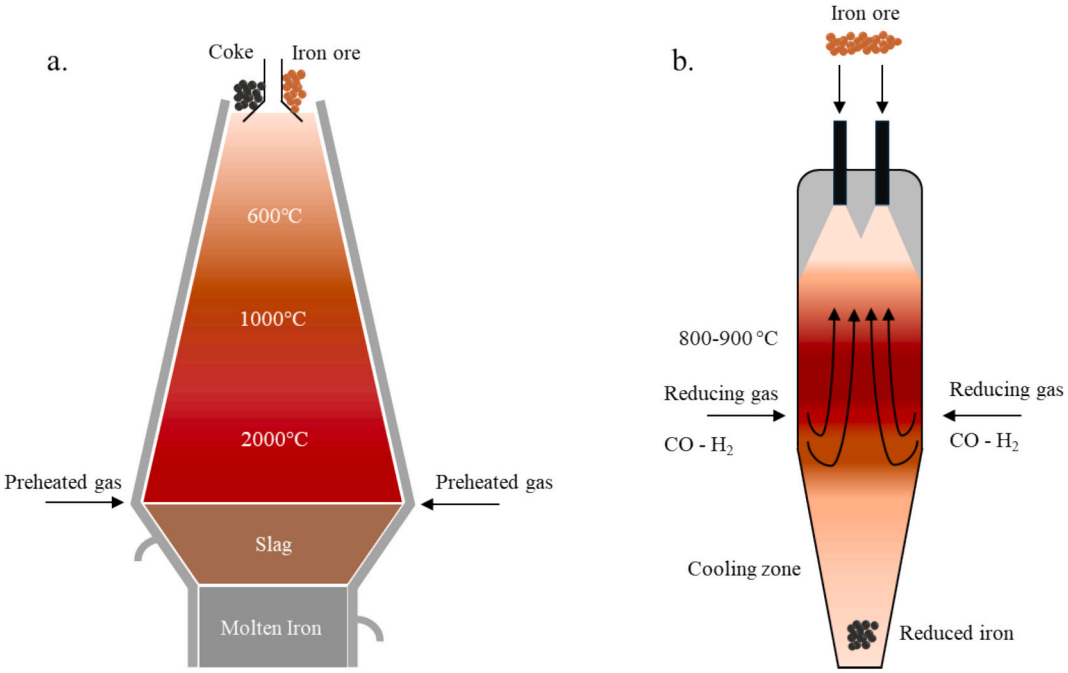

Fig. 1. Representative schemes of a) blast furnace and b) shaft furnace.

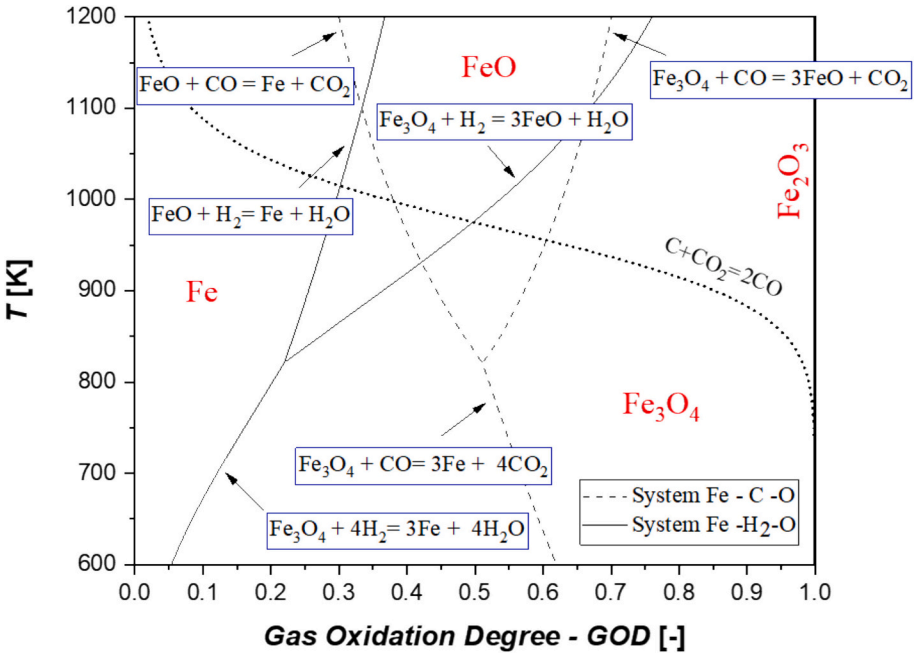

Fig. 3. Baur-Glässner diagram for Fe-C-O and Fe-H_2-O including Boudouard reaction, calculated by Fact Sage 8.2 [5].

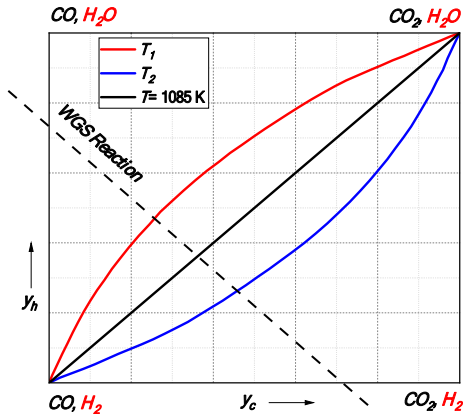

Fig. 4. Water gas shift equilibrium diagram calculated with Fact Sage 8.2 [5] varying temperatures at different hydrogen and carbon molar amount.

reaction, y_c and y_h, defined starting from the partial pressure of the different species

$$y_c = \frac{p_{CO_2}}{p_{CO_2} + p_{CO}} \tag{5}$$

$$y_h = \frac{p_{H_2O}}{p_{H_2O} + p_{H_2}} \tag{6}$$

The dashed line is thermodynamically used to determine the equilibrium state of the gas mixture at the specified temperature by locating its intersection with the equilibrium boundary. The intersection points give the gas compositions satisfying the equilibrium condition for the reaction at the specified temperature. From the diagram, it is clear that the equilibrium of this reaction strongly depends not only on temperature but also on the composition of the gas mixture that changes when the reaction occurs, as does the GOD. Moreover, it is reported in literature that various iron oxides, i.e., magnetite, wüstite, and also metallic iron catalyze the forward and reverse WGS. Other secondary reactions that can occur during the reduction are

$$C + H_2O \rightleftarrows CO + H_2 \tag{7.a}$$

$$3Fe + H_2 + CO \rightleftarrows Fe_3C + H_2O \tag{7.b}$$

$$CO + 3H_2 \rightleftarrows CH_4 + H_2O \tag{7.c}$$

$$2CO + 2H_2 \rightleftarrows CH_4 + CO_2 \tag{7.d}$$

$$Fe_2O_3 + 3CH_4 \rightleftarrows 2Fe + 6H_2 + 3CO \tag{7.e}$$

$$3Fe + CH_4 \rightleftarrows Fe_3C + 2H_2 \tag{7.f}$$

The multitude of reaction routes and the catalytic influence of iron and iron oxide phases coupled with thermodynamic aspects make the overall reaction network and factors affecting the kinetics rather complex. Moreover, the reduction kinetics of iron oxides are strongly influenced by pore structure, particle morphology, and gas accessibility, which governs the transport of reducing gases and the evolution of reaction interfaces [22]. In this work, the intrinsic kinetics of iron oxide reduction for pure material and for powder produced from both blast furnace and direct reduction pellets, have been studied. The experimental setup used to conduct the study enables following the off-gas composition online, which differs from the frequently used gravimetric methods reported in literature. Furthermore, the present study combines off-gas analysis with SEM and CHNS characterization to correlate reduction kinetics, carbon deposition, and microstructural evolution. It presents a novel approach for estimating the degree reduction based on elemental gas balances and carbon deposition measurement. The thin-layer configuration minimizes mass transport limitations, enabling the intrinsic reduction mechanisms to be isolated and providing high-quality kinetic data for the development and validation of future models applicable to low-carbon direct reduction technologies. Several kinetic models have been developed for hydrogen reduction of iron oxide pellets; however, their applicability to mixed H_2–CO atmospheres remain limited due to the additional complexity introduced by simultaneous reduction pathways and gas interactions [23,24]. Although industrial processes operate on pellets, such fundamental kinetic information is an essential prerequisite for multiscale reactor and pellet modeling and for future optimization. These provide new insights into the coupled effects of gas composition, temperature, and material characteristics on the reduction behavior of iron-bearing materials under H_2/CO atmospheres. It should also be noted that

single pellet-scale experiments are problematic in the sense that individual pellets may have different compositions, degree of sintering, etc., so general conclusions may be hard to draw without making numerous reduction test of different pellets. Pellet powder, in turn, can be ground from several pellets and then properly mixed, therefore better reflecting the overall material. Furthermore, the initial composition of single pellets cannot be determined without destroying the structure, but samples of powders can be readily analyzed.

2. Materials and methods

2.1. Materials

Pure hematite ($\geq$ 96%) was purchased from Sigma Aldrich (CAS: 1309-37-1). Commercial BF and DR pellets were provided by steelmaking companies. The pellets were crushed and subsequently sieved using an AS200 sieve produced by Retsch GmbH in order to obtain fine powders of dimensions comparable to that of the pure material. The minimum range of particle diameter selected was 38 μm $< D_p <$ 53 μm. The gases (hydrogen, carbon monoxide, and helium, > 99.99%) were purchased from Woikoski Oy, Finland.

2.2. Chemical physical characterization

XRD analysis is a useful technique that provides information about physical properties or phase composition of powders. In this work, it proved useful not only to detect the initial differences between the composition of pure and commercial powders, but also to follow the reaction progress and the influence of side reactions. The instrument was a Panalytical Empyrean diffractometer that used a CuK_α (1.5418 Å) source and PIXcel 3D detector. The intensity was collected in a range between 20° and 80°. The spectra were analyzed with HighScore Plus program using ICDD power diffraction file library 2025 (PDF5+ 2025). CHNS analysis was used to quantify the amounts of carbon, hydrogen, nitrogen and sulfur in the solid phase. SEM imaging was essential to examine morphology and surface characteristics of the samples. The equipment used was a NovaNanoSem 450 FEI featuring a TLD detector.

2.3. Experimental set-up

In literature, gravimetrical methods have often been used to determine mass loss and to calculate the degree of reduction in reduction experiments of iron ore. The contributions of the different side reactions and the difficulty to discretize between their contribution to the overall reduction have likely contributed to the large scatter and contradictory results and interpretations reported in the literature. Instead of the classical approaches, in this work an experimental setup as displayed in Fig. 5 was used. The system consists of gas sources (cylinders), piping with valves and three flowmeters, a glass reactor in a furnace, a water trap, and a micro-GC. The ceramic furnace first heats the sample with a temperature ramp (here 10 °C/min) until the desired temperature is reached, after this maintaining isothermal conditions. A thermocouple is placed inside the reactor, and the temperature is constantly monitored during the heating and reaction phases. The flowmeters have a range between 0 and 2000 cm^3/min to provide a steady flow of hydrogen, carbon monoxide, and helium to the reactor. The reactor has a radius of $r_c = 15$ mm and a total length of $L = 15$ cm. The small sample of powder is placed on a porous quartz disk in the reactor to assure a flat and horizontal layer of the iron oxide sample (with a thickness of 0.5–1.0 mm). Below the plug, quartz wool is used to trap possible dust flowing with the gas to protect the detector. The off gases coming from the reactor pass through a water trap to remove water before the micro-GC. This experimental setup showed good reproducibility and high accuracy in analysis of the off-gas composition. In the experiments, different ratios of the reductants (H_2 and CO) were applied. For the present system, the estimated value of Weisz Prater criterion << 1 suggests that there are no diffusion limitations in the particles. A Thiele modulus of $\Phi < 1$ and effectiveness factor of $\eta \approx 1$ confirm that intraparticle diffusion is negligible. From a thermal point of view, a Biot number of Bi <0.1 suggests that the system is essentially isothermal. The residential time distribution (RTD) was determined for all the flowrates at different temperatures of the tests. An example of the fitting is reported in supporting information (Fig. S3). The results yield a Peclet number in the range $Pe = 70\ldots80$, meaning that the system is in the kinetic regime.

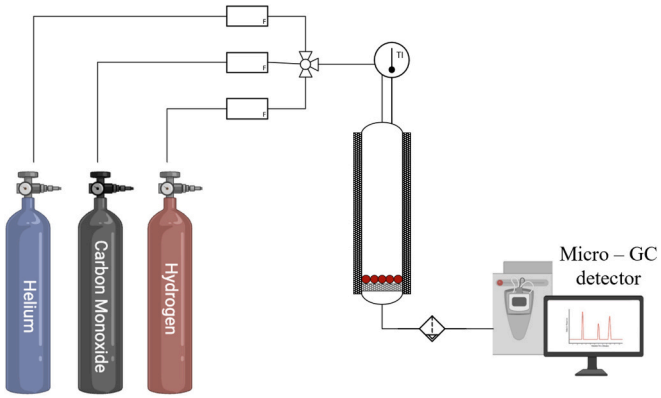

Fig. 5. Schematic of the experimental setup.

The influence of experimental parameters such as temperature (T), feed gas flow rate (Q), reductant percentage (Ψ), and reductant ratio H_2/CO on the reduction kinetics was investigated. The experimental matrix is reported in Table 1.

The fluid dynamics of the reactor were evaluated considering the different flow rates and temperatures. The residence time distribution was determined by step experiments for both hydrogen and carbon monoxide and the results were subsequently fitted using an unsteady state mass balance model with open-open vessel as boundary conditions. A mean estimated Peclet number of $Pe \approx 65$ and residence time of $\tau =$ 1.7 min show that complete plug flow is not quite achieved, even though advection is clearly dominating over diffusion. All the experiments were repeated three times to evaluate the repeatability and reproducibility of the data. In all cases, the curves obtained were superimposable, and the standard deviation associated was $\sigma < 5\%$.

3. Experimental results

3.1. Materials characterization

XRD patterns of the initial materials, displayed in Supporting material Fig. S.1, reflect the different composition between pure iron oxide and commercial pellet powders. Specifically, all the materials match with PDF no.00–033-0664 [36] corresponding to the spectra of pure hematite that crystallize in rhombohedral structure in the space group R-3c, with the lattice parameters $a = 5.035$ Å, $b = 5.035$ Å, $c = 13.7540$ Å, $\alpha = 90°$, $\beta = 90°$ and $\gamma = 120°$. Moreover, BF pellet powder contains two reflections at $2\Theta = 21°$ and $2\Theta = 27°$ that match with PDF no. 00–046-1045 [36] corresponding to the spectra of silicon oxide that crystallizes in rhombohedral structure in the space group $P3_221$, with the lattice parameters $a = 4.914$ Å, $b = 4.914$ Å, $c = 113.060$ Å, $\alpha = 90°$, $\beta = 90°$ and $\gamma = 120°$. Silicon oxide, or silica, like other oxides such as magnesium or manganese oxides is generally present as impurities called gangue. Table 2 reports the detailed compositions of BF and DR pellet powders.

SEM analysis reveals important morphological differences as shown in Fig. 6. The pure material appears organized, with alternating agglomeration of small grains and voids between the particles. BF pellet powder appears a dense and non-porous material with a sintered surface. DR pellet powder displays blended morphological organization

Table 1
Experimental matrix of experiments for a) pure hematite and b) commercial powders.

a. Pure hematite	T [°C]	Q [mL/min] ([mL/min]	Ψ [%]	H_2/CO [−]	m [g]	D_p [μm]
Temperature	600	80	25%	1/1	0.100	< 5
	800	80	25%	1/1	0.100	< 5
	1000	80	25%	1/1	0.100	< 5
	600	40	25%	1/1	0.100	< 5
Total flow rate	600	80	25%	1/1	0.100	< 5
	600	120	25%	1/1	0.100	< 5
	600	80	25%	1/1	0.100	< 5
Reductant percentage	600	80	50%	1/1	0.100	< 5
	600	80	75%	1/1	0.100	< 5
	600	80	25%	3/1	0.100	< 5
Reductant ratio	600	80	25%	1/3	0.100	< 5
b. BF/DRI pellet powder						
	600	80	25%	1/1	0.100	38 μm - 53 μm
	800	80	25%	1/1	0.100	38 μm - 53 μm
Temperature	1000	80	25%	1/1	0.100	38 μm - 53 μm
	600	40	25%	1/1	0.100	38 μm - 53 μm
Total flow rate	600	80	25%	1/1	0.100	38 μm - 53 μm
	600	120	25%	1/1	0.100	38 μm - 53 μm
	600	80	25%	1/1	0.100	38 μm - 53 μm
Reductant percentage	600	80	50%	1/1	0.100	38 μm - 53 μm
	600	80	75%	1/1	0.100	38 μm - 53 μm
	600	80	25%	3/1	0.100	38 μm - 53 μm
Reductant ratio	600	80	25%	1/3	0.100	38 μm - 53 μm

composed of partially agglomerated grains, voids and sintered surfaces, which likely is the result of a lower temperature of pretreatment. Nitrogen physisorption confirmed relatively low specific surface areas of about 7 m^2/g for pure hematite and 1 m^2/g and 0.2 m^2/g for DR and BF pellet powders, respectively [24]. DLS analysis of the particle sizes resulted in average values of 10 μm for pure hematite and 30 μm for the commercial samples [25]. The present work employs nitrogen physisorption and DLS to characterize the powder, but in the future more sophisticated techniques could be used. For instance, recent three-dimensional imaging studies by Cavaliere et al. [26] have demonstrated the importance of pore connectivity and morphology in controlling reducibility.

3.2. Morphological conversion during the reaction

As demonstrated by D'Angelo et al. [24,25], morphology contributes significantly to the overall reduction kinetics when pure hydrogen or carbon monoxide is used as the reductant. High temperature ramps were observed to promote sintering and agglomeration of the particles of pure hematite and fracturing of the surface of the commercial samples, related to the decomposition of hematite

$$Fe_2O_3 \rightleftarrows 4Fe_3O_4 + O_2 \quad (8)$$

Subsequently, SEM, XRD and CHNS analyses were performed at the reaction times of $t = 5$ min, $t = 10$ min, $t = 50$ min. The experiments were conducted at $T = 600$ °C, a total gas flow rate of $Q = 80$ mL/min, a reductant percentage of $\psi = 25\%$ with a hydrogen-to-carbon monoxide ratio of $H_2/CO = 1/1$.

The evolution of the XRD spectra during the reaction for pure and commercial materials is presented in Fig. 7. The reflections move across the three iron oxides phases from hematite to wüstite. Iron formation occurred faster in gas mixtures compared to pure hydrogen and carbon monoxide for BF and DR pellet powders. Moreover, these analyses also confirm and reflect the effects of the reverse Boudouard reaction. Specifically, it is possible to observe the simultaneous presence of the reflections related to carbon deposition and cementite formation at $t = 150$ min and $t = 50$ min for pure hematite and the commercial materials, respectively.

A comparison of SEM images for pure hematite at different reaction times using different reducing agents is provided in Fig. 8. The microstructural changes due to the conversion of phases coupled with the increase in pore and small grain formation, lead to the production of sponge iron in hydrogen reduction. The observed increase in porosity during reduction is consistent with the findings from previous studies of hydrogen reduction of iron oxide pellets, where pore evolution significantly affected gas diffusion and reduction kinetics [27]. The increase in porosity observed during reduction can be attributed to the progressive removal of oxygen from the iron oxide lattice and the associated volume changes accompanying the phase transformations. The newly formed pore network facilitates the diffusion of reducing gases toward the unreacted core, simultaneously promoting the outward transport of the gaseous reaction products. Similar observations have been reported for hydrogen reduction of iron oxide pellets, where pore development was

Table 2
Chemical composition of the BF and DR pellets.

	Fe [%]	FeO [%]	Al_2O_3 [%]	CaO [%]	MgO [%]	MnO [%]	SiO_2 [%]
BF pellet	64.9	0.15	0.34	1.04	0.39	0.15	5
DR pellet	66.9	0.69	0.43	0.99	0.28	0.053	1.73

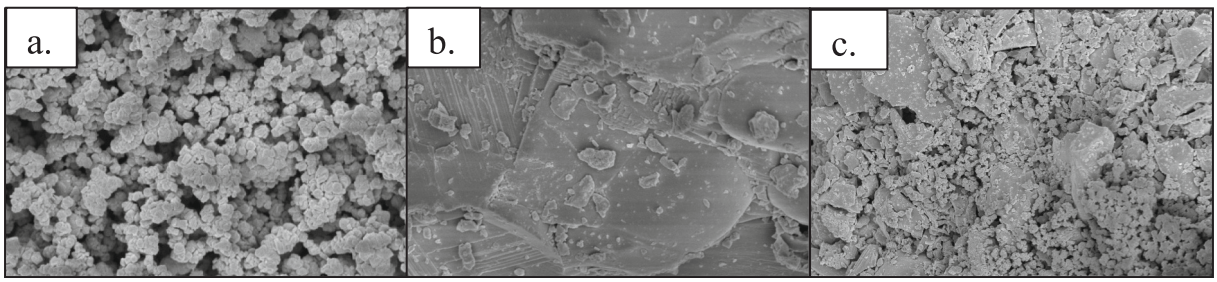

Fig. 6. SEM images at time $t = 0$ min of a) Pure hematite, b) BF pellet powder, c) DR pellet powder.

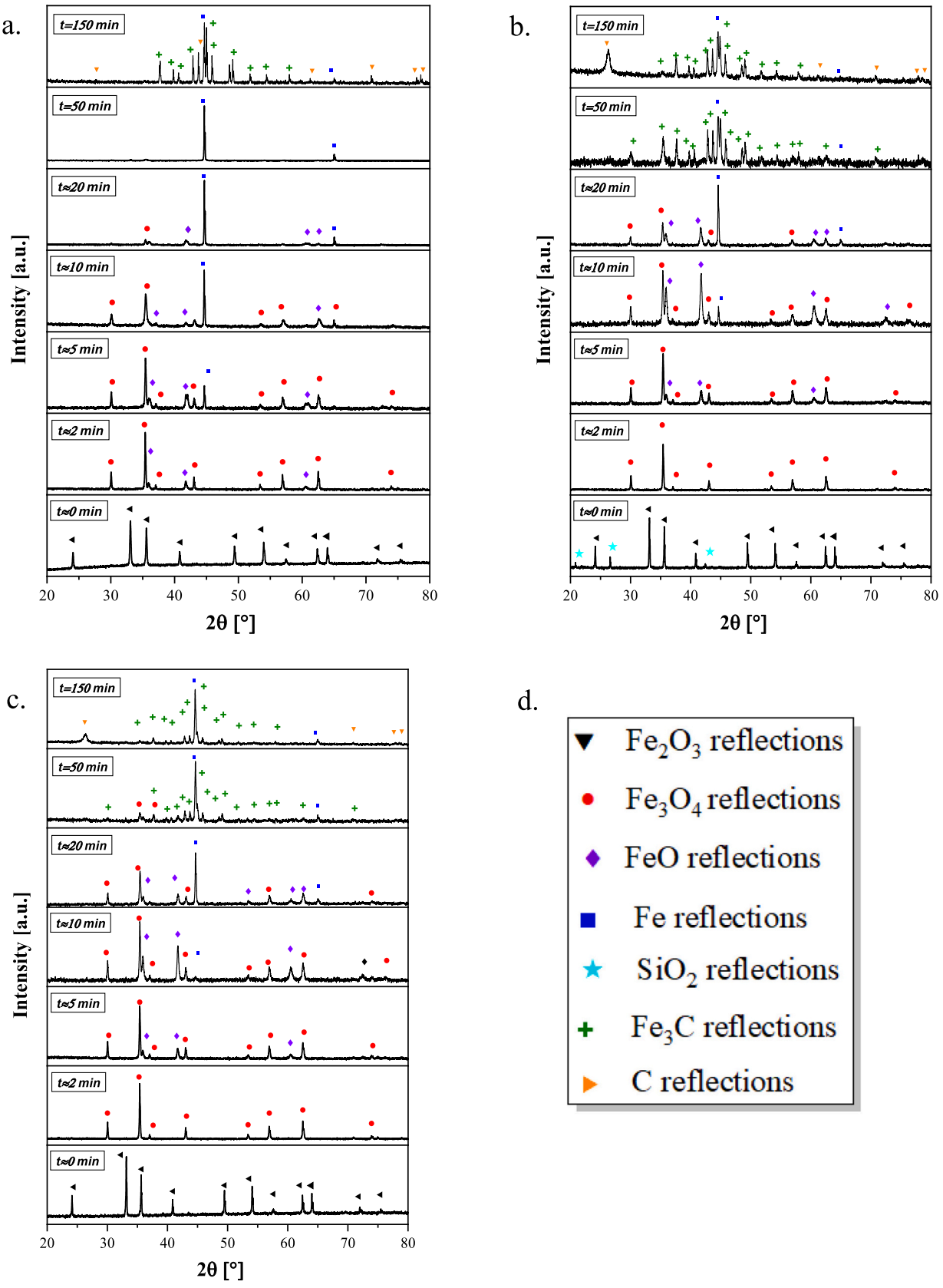

Fig. 7. XRD analyses at different reaction time for a) pure hematite, b) BF pellet powder, c) DR pellet powder [25].

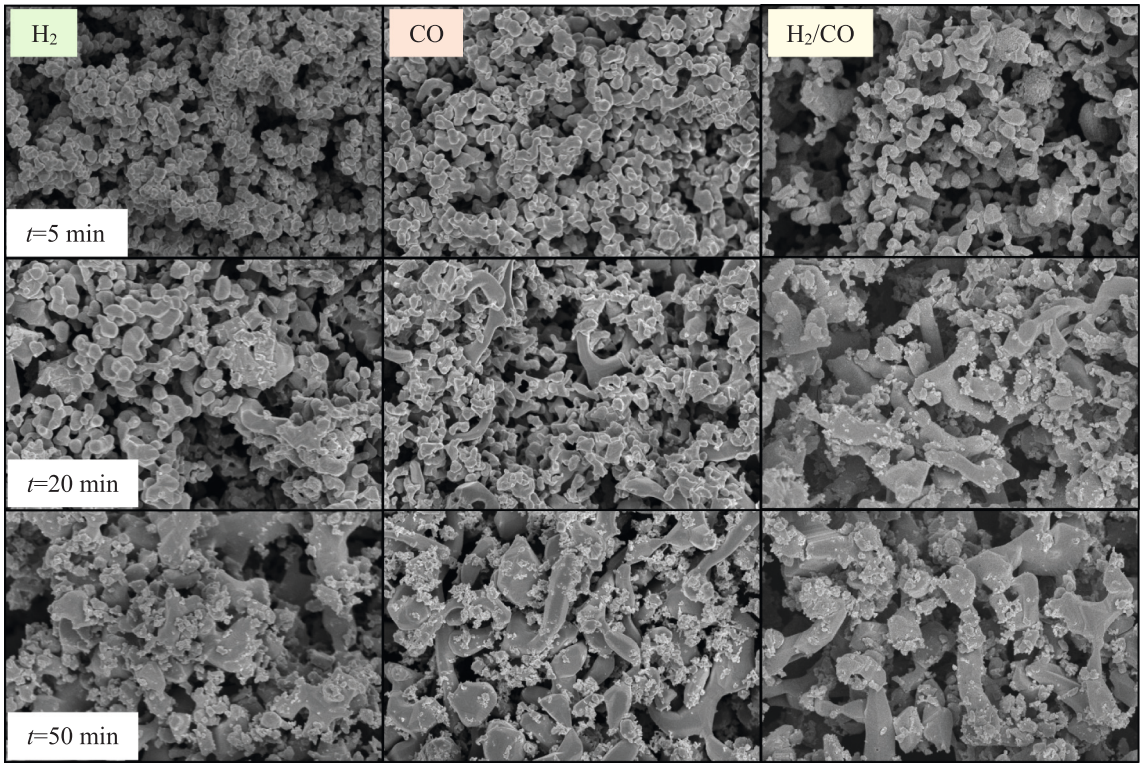

Fig. 8. SEM images of pure hematite at different reaction times (Q = 80 mL/min and T = 600 °C). H_2: y_{H2} = 0.25, CO: y_{CO} = 0.25, and H_2/CO: y_{red} = 0.25, H_2:CO = 1:1.

identified as a key factor controlling reduction kinetics [28]. This is consistent with the evolution observed by nitrogen physisorption, reported in Fig. S2. The reduction by carbon monoxide exhibits a heterogeneous mix of porous dark and dense grains, and porous bright regions, indicating the presence of metallic iron. Specifically, it is possible to observe fibrous structures of iron particles that appear as

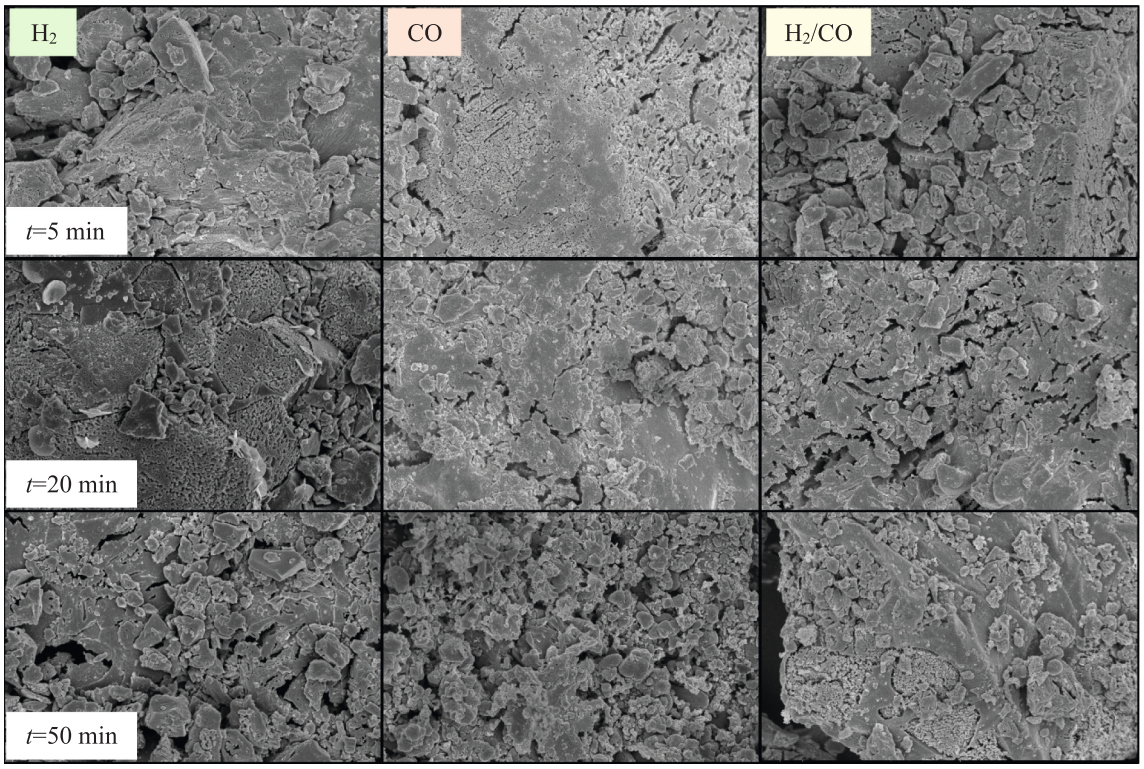

Fig. 9. SEM images of BF pellets at different reaction times (Q = 80 mL/min and T = 600 °C).
H_2: y_{H2} = 0.25, CO: y_{CO} = 0.25, and H_2/CO: y_{red} = 0.25, H_2:CO = 1:1.

typical iron whiskers, i.e., filaments that grow on the surface, and small agglomerated islands that correspond to carbon deposition. A combination of these explains the morphological changes for experiments with both H_2 and CO in the gas.

Compared to pure materials, BF and DR pellet powders (Figs. 9 and 10) exhibit more complex microstructures that combine the evolution of particles and surface morphology. In the first case, while hydrogen reacts, the evolution of a sintered and dense material with cracks and grain formation on the surface was observed. The reduction with carbon monoxide, in turn, resulted in a distinct layer formation, tending to lead to a porous iron with significant pore growth and potentially enhanced deposition of carbon, which was confirmed by XRD and CHNS analysis. The results are discussed in more detail in the next section. The combination of hydrogen and carbon monoxide enhances these characteristics, with H_2 generally promoting a more homogeneous, sponge-like metallic iron structure and CO tending to yield larger pore diameters, thereby influencing surface area and morphology through carbon content.

3.3. Reduction kinetics

Next, the effect of different experimental conditions on the iron oxides kinetics using a mixture of hydrogen and carbon monoxide as reducing agents was investigated. The results of an experiment conducted at a total flowrate of $Q = 80$ mL/min, a temperature of $T = 873$ K, a total reductant percentage of $\psi = 25\%$ and equal amounts of H_2 and CO (H_2:CO = 1:1) are displayed in Fig. 11.a, b and c for pure hematite, BF, and DR pellet powders, respectively. The area that are detectable by micro-GC are converted into the gas molar ratio of various species. It represents the trend of the off gases at the exit of the reactor. Initially, during the fast hematite reaction, low amounts of reducing gases are observed in the outflow because they are consumed, but the signal for CO and H_2 subsequently gradually approach the inlet molar ratio to reach this level when the reduction reactions are finished. The hydrogen ratio in the outflowing gases exhibits a similar behavior as has been observed by the present authors in earlier work [22,23,29,30,31]. For pure hematite, the changes in the slope of the gas concentration curves reflect the different and consecutive reaction phases until metallic iron is formed. For the samples of commercial materials, the presence of a minimum in hydrogen ratio is due to the formation of cracks on the surface, exposing fresh surfaces and increasing the reduction reaction rates. After 20 min, the hydrogen consumption remains almost constant, approaching the third stage of the reduction reactions. This is supported by findings from the XRD analysis, as iron reflections appear from this point onwards. The water content is not directly measured but can be calculated from a hydrogen balance of the gas. Hydrogen consumption provides a direct estimate of the stoichiometric amount of water that could be formed during the reduction process if all hydrogen reacts to form water, that is $\dot{n}_{H_2O} = 0.45$ mmol/min. On other hand, at a temperature of 873 K, the water gas shift reaction equilibrium constant is $K_{WGS} \approx 2.7$ and the equilibrium molar flow of water (vapor) that would be attended is $\dot{n}_{H_2O} = 5.7{\cdot}10^{-2}$ mmol/min. This deviation between the two values indicating that thermodynamic equilibrium for the WGSR was not attained under the investigated conditions and that the reaction behavior was kinetically controlled, so the reaction is in the kinetic regime. In the late stage of the reaction, the experimental trends are consistent with what would be expected if the water-gas shift (WGS) reaction progresses toward chemical equilibrium. However, under the present experimental conditions, the process remains in the kinetic regime, and no assumption is made that chemical equilibrium of the WGS reaction is attained.

The carbon monoxide and carbon dioxide curves display mirror trends that correspond to different stages of reduction. At the beginning, most of the H_2 and CO are consumed in the rapid hematite reduction reaction, but their concentrations sharply increase after the hematite is reduced. Previous studies have demonstrated that H_2 shows faster intrinsic reduction kinetics and diffuses more readily through the porous product layer, whereas CO follows a different reduction pathway and

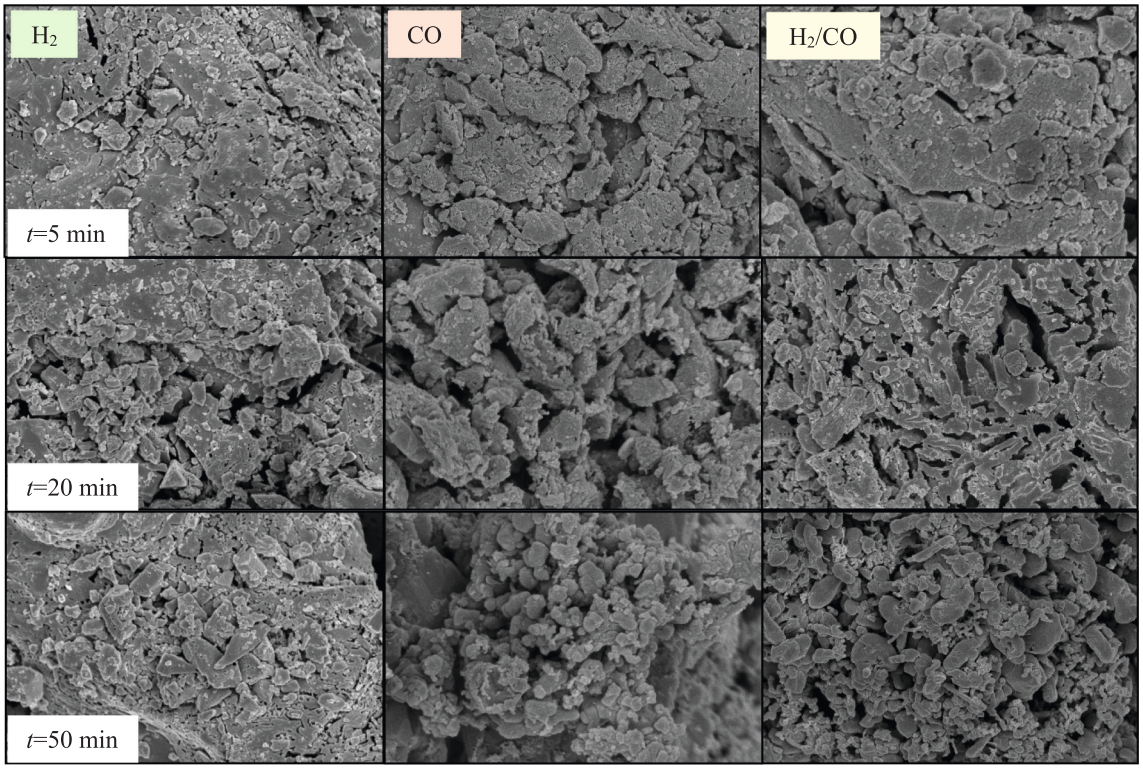

Fig. 10. SEM images of DR pellets at different reaction times ($Q = 80$ mL/min and $T = 600$ °C).
H_2: $y_{H2} = 0.25$, CO: $y_{CO} = 0.25$, and H_2/CO: $y_{red} = 0.25$, H_2:CO = 1:1.

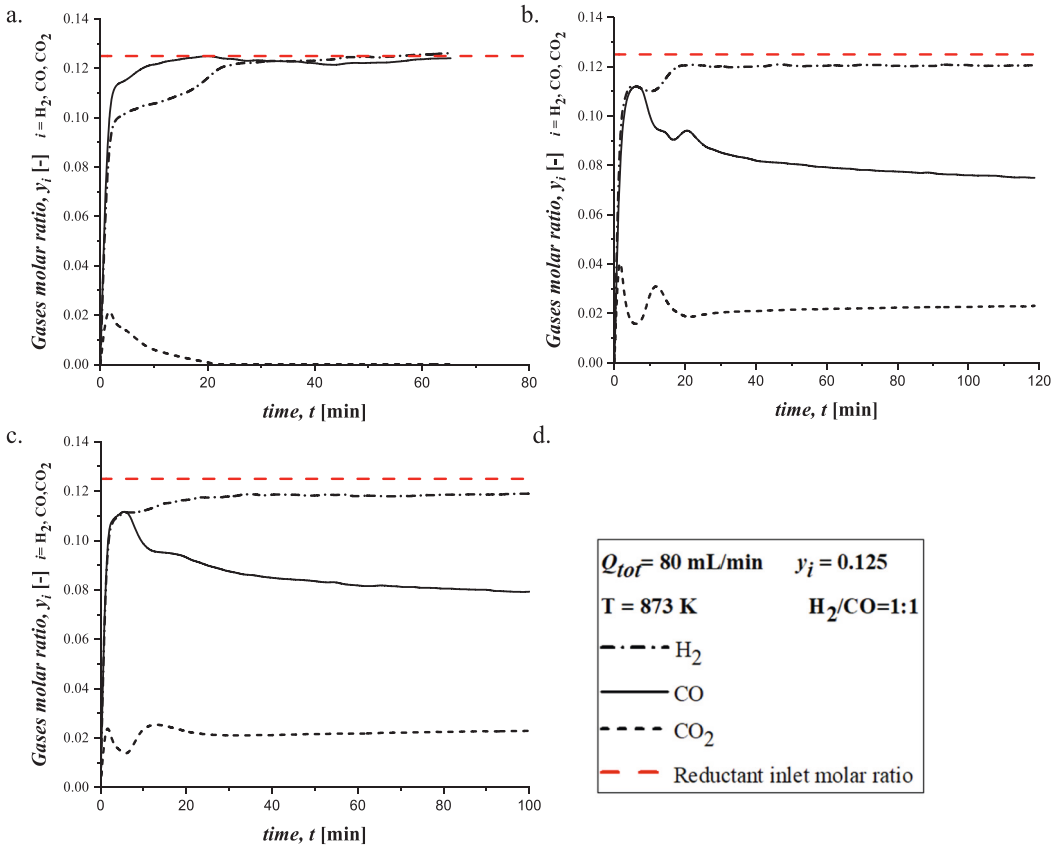

Fig. 11. Molar ratios of hydrogen, carbon monoxide and carbon dioxide for reduction experiments at $T = 600$ °C, $Q = 80$ mL/min, $y_i = 0.125$ and $H_2/CO = 1:1$ for a) Pure hematite, b) BF pellet powder, and c) DR pellet powder. The inlet molar ratio of the reductants is depicted by the red dashed line. Experimental reproducibility was evaluated by three independent experiments. The corresponding 95% confidence intervals are smaller than the graphical resolution of the figure (relative uncertainty <5%), so error bars are omitted for clarity.

exhibits stronger adsorption on hematite surfaces. Furthermore, H_2-rich atmospheres have been reported to promote the development of a more porous reduced layer, facilitating gas transport and sustaining rapid reduction conditions. The coexistence of H_2 and CO may therefore modify surface coverage and the availability of active sites, leading to more efficient oxygen removal than for either reducing gas alone [32,33]. The enhanced reduction in mixed H_2 and CO atmospheres may arise from the different elementary reaction pathways of H_2 and CO on hematite surfaces, allowing complementary oxygen removal mechanisms. Recent DFT calculations have shown that H_2 and CO exhibit different adsorption strengths on hematite surfaces, while the adsorption of reaction products (H_2O and CO_2) further modifies the adsorption behavior of the reducing gases, influencing the interfacial reaction kinetics [34,35]. The hydrogen consumption then follows the magnetite-wustite-iron pathway with declining order in reaction rate. After the hematite reduction, the CO concentration, on the other hand, starts declining to finally level out (at an apparently steady state). This behavior can be explained by the reverse Boudouard reaction that decomposes CO, forming elemental carbon and CO_2. CO_2 increases in the early and intermediate stages of the reduction and finally approaches a plateau. There is a clear difference in this trend and in the obtained steady state composition between the pure hematite and the commercial samples, indicating a much stronger reverse Boudouard reaction for the latter ones. This aspect is discussed in the next paragraph.

3.4. Reverse boudouard reaction and carbon deposition

The reverse Boudouard reaction may be catalyzed by iron and different oxides, e.g., iron oxides, silicon oxide, and aluminum oxides. The carbon deposition is strongly influenced by the temperature at which the reduction process is performed and by the composition of the gas mixture. During the reaction, reduction and carbon deposition may occur simultaneously according to the equilibria presented in the Baur-Glässner diagram (Fig. 3). At the beginning of the process, the reduction is the predominating reaction, and the based on the XRD analysis, cementite and carbon were detected only later in the experiments, $t >$ 20 min. This may be due to the presence of sufficient amounts of water vapor, which has been found to retard or fully prevent reverse Boudouard reaction [36]. At this stage, the iron formed, react with the elemental producing iron carbide (cementite) according to Eq. (7.b). The cementite continues to grow on the surface of the particles and after a while, the whole surface is covered by it, slowing down the diffusion of the reducing gas. At this stage, carbon starts depositing on this layer, also reacting with unreacted oxides present inside the particles. An apparent steady state is established, seen as plateaus in the molar ratios of the outflowing gas. The layer-forming process is schematically depicted in Fig. 12.

To interpret the decrease of the CO concentration noted above and to explain the difference in the behavior of the pure and commercial material, CHNS quantification analysis was performed. This technique was applied to determine the amount of carbon deposited at various reaction times for various experiments to gain information about the carbon deposition mechanism. Fig. 13 reports the amount of deposited carbon for pure and commercial samples of the experiments of Fig. 11 (conducted at $Q = 80$ mL/min, $T = 873$ K, $\psi = 25\%$, and H_2:CO = 1:1). The differences in the carbon content of BF and DR pellet powder are so small that the right panel represent both materials. The results show that the carbon deposition subsequently to carbide formation would follow

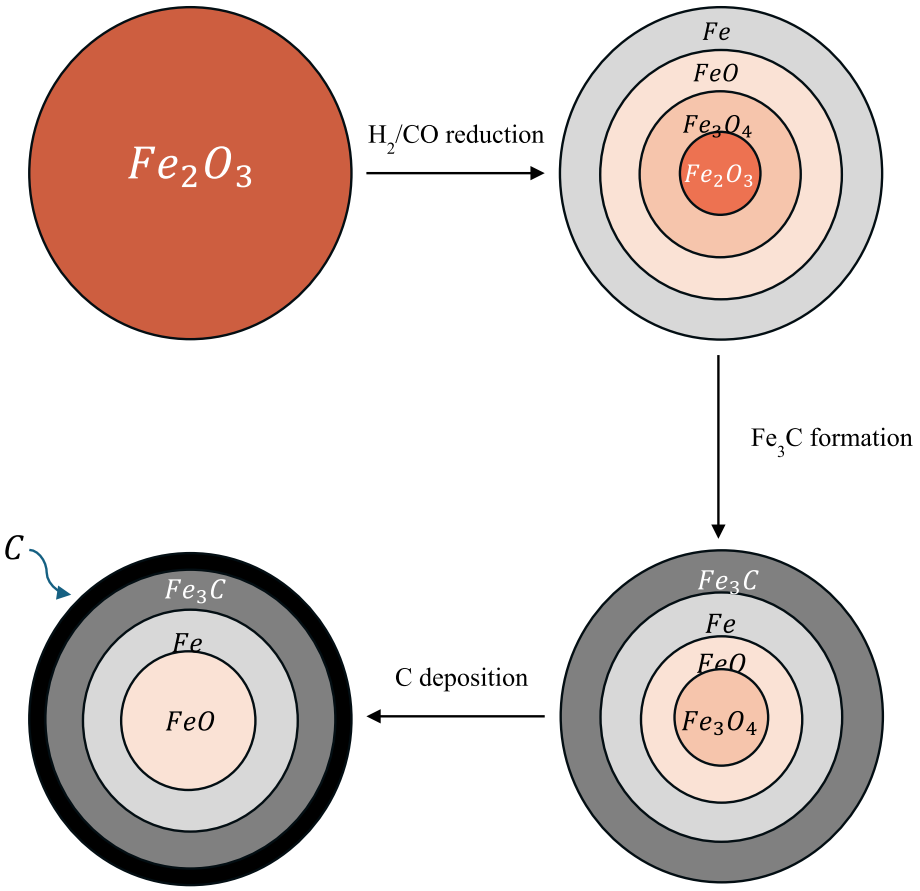

Fig. 12. Schematic of reduction, cementite formation and carbon deposition.

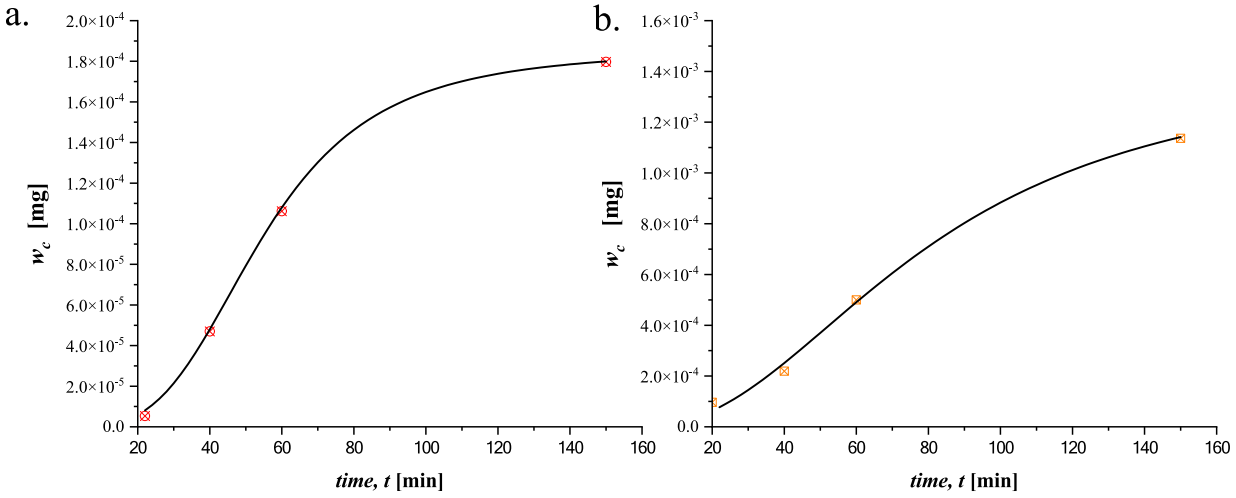

Fig. 13. Carbon deposition amount for an experiment with $Q = 80$ mL/min, $T = 873$ K, $\psi = 25\%$, and H_2:CO = 1:1 for a) pure hematite, b) BF and DR pellet powders measured by CHNS analysis (red squares) and approximated by the Langmuir equation.

the Langmuir adsorption equation that is broadly used to describe gas adsorption on solids. It is obtained by the interpolation of the data. The mechanistic investigation of carbon formation using DFT calculation developed by Lu et al. [37,38] suggested that the process involves the adsorption of carbon monoxide on the iron surface, bond stretching due to the attractive force of Fe, and finally the conversion due to the presence of CO and H_2 molecules. The carbon weight obtained in Fig. 13 for both materials were obtained by analyzing an average 2 mg of samples in CHNS.

The carbon deposition was estimated for experiments conducted at different temperatures, flow rate, reductant percentage and ratio, for all the three sample materials. According to the Baur-Glässner plot, lower temperature promotes the reverse Boudouard reaction, so lower concentrations of CO are needed to trigger carbon deposition. Moreover, it is well known that the presence of hydrogen promotes carbon deposition because it decreases the activation and adsorption energy but, as expected, for higher hydrogen concentrations (and lower CO concentration) the amount of deposited carbon radically decreases. This effect is

reported in Fig. 14, where the influence of hydrogen on the carbon mass deposition percentage, calculated as mass of carbon divided by the mass of the initial sample analyzed, is displayed for tests conducted at $T = 873$ K, a total flow rate of $Q = 80$ mL/min, and reductant percentage of $\psi = 25\%$. The stronger apparent reverse Boudouard activity observed for the commercial samples suggests that material-specific properties govern the extent of CO disproportionation under the investigated conditions. The marked difference in carbon concentration between materials is attributable to the combination of composition and morphology of commercial samples. The presence of gangue affects this phenomenon, where alumina and silica promote deposition [38]. Previous investigations have shown that gangue constituents and minor oxides, such as TiO_2, can significantly modify hydrogen reduction behavior and subsequent carburization of industrial pellets [23]. Finally, the more severe carbon deposition observed for BF and DR pellet powders suggests that industrial iron-bearing materials may be more susceptible to permeability loss than pure hematite. This can also increase pressure drop, reduce bed permeability, and deteriorate heat transfer. However, the reactor scale, the amount of pellet powders and the low gas flowrate used in this work avoid heat and pressure gradients.

To theoretically study the role of the higher deposition promoted by gangue, simulations of the conditions in the later stages ($t > 20$ min) of the reduction experiments were undertaken, where the initial iron oxide reduction was neglected since the fast reduction was assumed to prevent carbon deposition, as suggested by the XRD analyses of the samples. Mass balance equations for oxygen carbon and hydrogen can be written

$$\dot{n}_{CO}^{in} = \dot{n}_{CO_2}^{out} + \dot{n}_{CO}^{out} + \dot{n}_{C}^{dep} \tag{9}$$

$$\dot{n}_{CO}^{in} + \dot{n}_{O}^{red} = \dot{n}_{CO}^{out} + 2\dot{n}_{CO_2}^{out} + \dot{n}_{H_2O}^{out} \tag{10}$$

$$2\dot{n}_{H_2}^{in} = 2\dot{n}_{H_2}^{out} + 2\dot{n}_{H_2O}^{out} \tag{11}$$

where superscripts "in" and "out" refer to the incoming and outgoing gases, "dep" to carbon deposition and "red" to (iron oxide) reduction. The model includes the carbon deposition rate ($\dot{n}_C^{dep}$) calculated from the experiments described above (cf. Fig. 13). Since the water content of the outgoing gas was not successfully determined in the experiments, the mass balance equations alone are insufficient to uniquely determine the outlet gas composition. Consequently, an additional relationship is required to close the system. In the present work, the thermodynamic equilibrium of the water–gas shift reaction was adopted as this closure relationship. The equilibrium assumption is supported by the comparatively fast kinetics of the water–gas shift reaction over iron and iron oxide surfaces. Numerous studies have reported that the characteristic time of the WGS reaction is considerably shorter than that of iron oxide reduction, making local thermodynamic equilibrium a reasonable approximation during the later stages of the experiments, where the outlet gas composition varied only slowly with time and XRD analysis indicated that the rapid reduction of hematite had essentially ceased. Under these quasi-steady conditions, the WGS equilibrium provides a reasonable approximation for estimating the unmeasured water concentration. For a given $\dot{n}_C^{dep}$, the model can calculate the composition of the gas that leaves the system (see the Appendix). The balance equation system offers an innovative way to estimate the change of the reduction degree. From Eq. (10), the reduction rate, i.e., removal rate of oxygen from the sample, can be expressed as

$$\dot{n}_{O}^{red} = -\dot{n}_{CO}^{in} + \dot{n}_{CO}^{out} + 2\dot{n}_{CO_2}^{out} + \dot{n}_{H_2O}^{out} \tag{12}$$

Combined with Eqs. (9) and (11), this gives

$$\dot{n}_{O}^{red} = \dot{n}_{CO_2}^{out} + \left(\dot{n}_{H_2}^{in} - \dot{n}_{H_2}^{out}\right) - \dot{n}_{C}^{red} \tag{13}$$

Thus, the reduction rate, i.e., change of the degree of reduction with time, can be expressed as

$$\frac{d\alpha}{dt} = \frac{\dot{n}_{CO_2}^{out} + \left(\dot{n}_{H_2}^{in} - \dot{n}_{H_2}^{out}\right) - \dot{n}_{C}^{red}}{n_{O}^{ini}} \tag{14}$$

where n_O^{ini} is the initial amount of (removable) oxygen in the iron oxide sample. By integrating this equation, the evolution of the estimated reduction degree can be followed during the experiments.

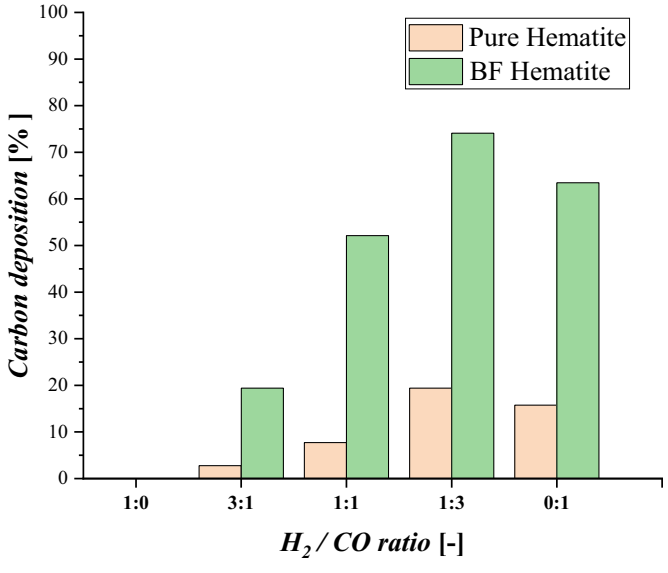

Fig. 14. Influence of the hydrogen-carbon monoxide ratio on the carbon deposition percentage for pure hematite and BF hematite. The carbon mass deposition ratio is defined as the ratio between the mass of the deposited carbon and the initial mass of the iron oxide sample.

3.5. Evolution of the reduction degree

As previously described, the test performed at $T = 600$ °C, $Q = 80$ mL/min, $m_{Fe2O3} = 0.1$ g, $y_{red} = 0.25$ and H_2/CO ratio 1:1 is considered the basepoint experiment. Generally, at the beginning, the reaction is chemically controlled by surface reaction of Fe_2O_3 that converts into Fe_3O_4. Afterwards, a slower dynamic are noted: wüstite reacting to form iron is generally reported to be the limiting reaction step. Moreover, diffusion through the different iron oxide layers coupled with the influence of the Boudouard reaction that starts to deposit carbon on the sample surface, water gas shift reaction and carbide formation that cover all the surface, decrease the final efficiency of reactions. Subsequently, the chemical results altering different experimental conditions has been calculated. Fig. 15 presents the estimated evolution of the reduction degree of pure hematite in hydrogen and carbon monoxide atmospheres at different temperatures (panel a), molar ratios of reductant in the feed gas (panel b), gas flow rates (panel c), and different H_2: CO ratios (panel d).

Temperature has a strong effect not only because it directly influences the reduction reaction rates but also because it reduces the stability region of carbon in the Boudouard reaction (cf. Fig. 3). Increasing the temperature from 873 K to 1273 K, the reaction rate increases, particularly between 873 K and 1073 K, decreasing the overall reaction time and approaching complete reduction ($\alpha = 1$) in about 20 min for the highest temperature studied. Additionally, CO reduction becomes increasingly favorable at higher temperatures because the endothermic Boudouard equilibrium shifts toward CO formation, maintaining reducing potential. As expected, increasing the reductant concentration (Fig. 15.b), the reaction becomes faster and the overall reduction time decreases. From a thermodynamic perspective, increasing reducing gas concentration lowers the oxygen partial

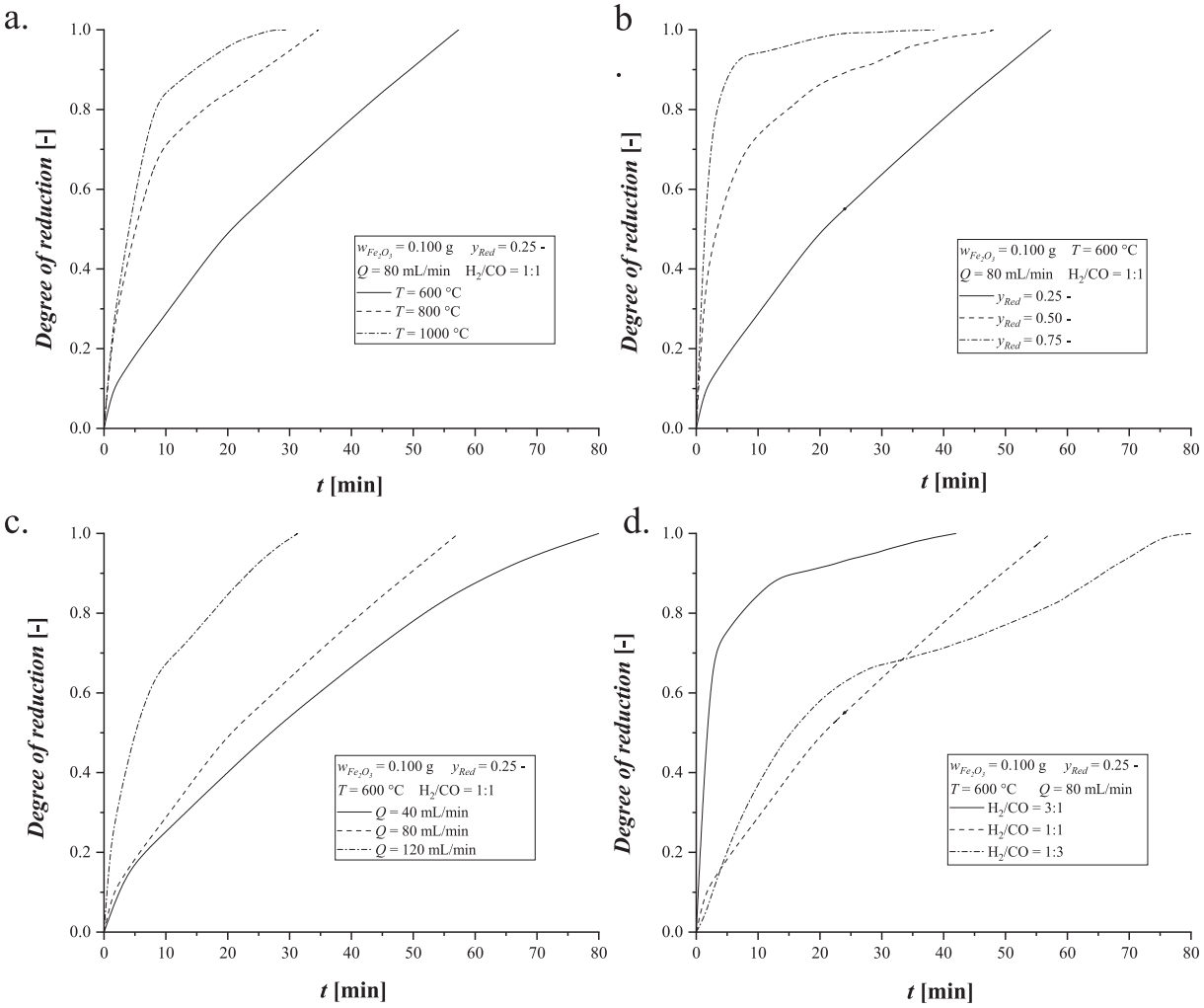

Fig. 15. Estimated reduction degree for pure hematite varying a) temperature, b) gas flow rate, c) molar ratio of reductants in the feed gas, and d) molar ratio between hydrogen and carbon monoxide. Experimental reproducibility was evaluated by three independent experiments. The corresponding 95% confidence intervals are smaller than the graphical resolution of the figure (relative uncertainty <5%), so error bars are omitted for clarity.

pressure in the reactor environment, shifting equilibrium toward metallic iron formation. An increase in the gas flow rate (Fig. 15.c) mitigates the effect of starvation of reductants and enhances the reactions. At low flow rates, accumulation of oxidized gaseous products may suppress reaction kinetics through equilibrium limitations. Increasing the flow rate enhances convective transport and minimizes concentration polarization near the solid surface. Finally, the molar ratio between hydrogen and carbon monoxide (Fig. 15.d) also plays an important role: The addition of hydrogen promotes the reaction, even though the driving force at this temperature (873 K) is lower for hydrogen than for carbon dioxide (Fig. 3): this can be ascribed to the better diffusion of the small H_2 molecules combined with suppression of the reverse Boudouard reaction. Some conflicting effects are observed in that the experiment with H_2:CO = 1:3 initially reduces faster that in the experiment with equal H_2 and CO, even though the time to full reduction is longer. Neither do the slope changes of the former experiment match what was observed for the other experiments of the study, which may be due to the overlapping of the reduction reaction steps or, possibly, some inconsistencies of the experiment in question. On other hand, the reduction behavior of powders of blast furnace and direct reduction pellets reported in Fig. 16 and Fig. 17 show clear differences compared to what was observed for pure hematite in Fig. 15. Generally, the reduction is slower except for at the highest temperature where the results are similar: at 1273 K, all samples are fully reduced within 20 min. At this temperature, the effect of carbon deposition is little. At 873 K, where the pure hematite approached full reduction after 60 min, the corresponding time for the DR and BF pellets are 80 min and > 140 min. Thus, the DR pellet acts as an intermediate between pure hematite and BF pellets, which is justified by the composition (Table 2). Increasing the molar ratio of reductant in the gas from 0.25 to 0.50 (Figs. 16.a and 17. b) has a smaller effect than for pure hematite, but an increase to 0.75 clearly shortens the time to reach full reduction. The effect of the gas flow rate is qualitatively similar for the hematite and BF pellet powders (Fig. 15.c and 16.c), but for DR pellets the results at $Q = 80$ mL/min and $Q = 120$ mL/min are almost identical (Fig. 17.c). Increasing the H_2:CO ratio is beneficial since it shortens the reduction time, but more linearly for DR than for BF pellet powders. This indicates that more hydrogen is needed to see a marked effect on the reduction of BF pellets (at this low temperature). Overall, the pellet powder curves often show clear slope changes, which usually match with the reduction degree of the main oxides. If the initial material is pure hematite, full reduction to magnetite or wustite would occur at $\alpha = 0.11$ and $\alpha = 0.33$ if the reactions in the sequence are not considered to overlap. The experimental results presented here also provide a useful dataset for assessing kinetic models describing iron oxide reduction under mixed H_2–CO atmospheres. Because the experiments were performed using a thin powder layer, external and internal diffusion effects were minimized, allowing the measured behavior to more closely represent the intrinsic gas–solid

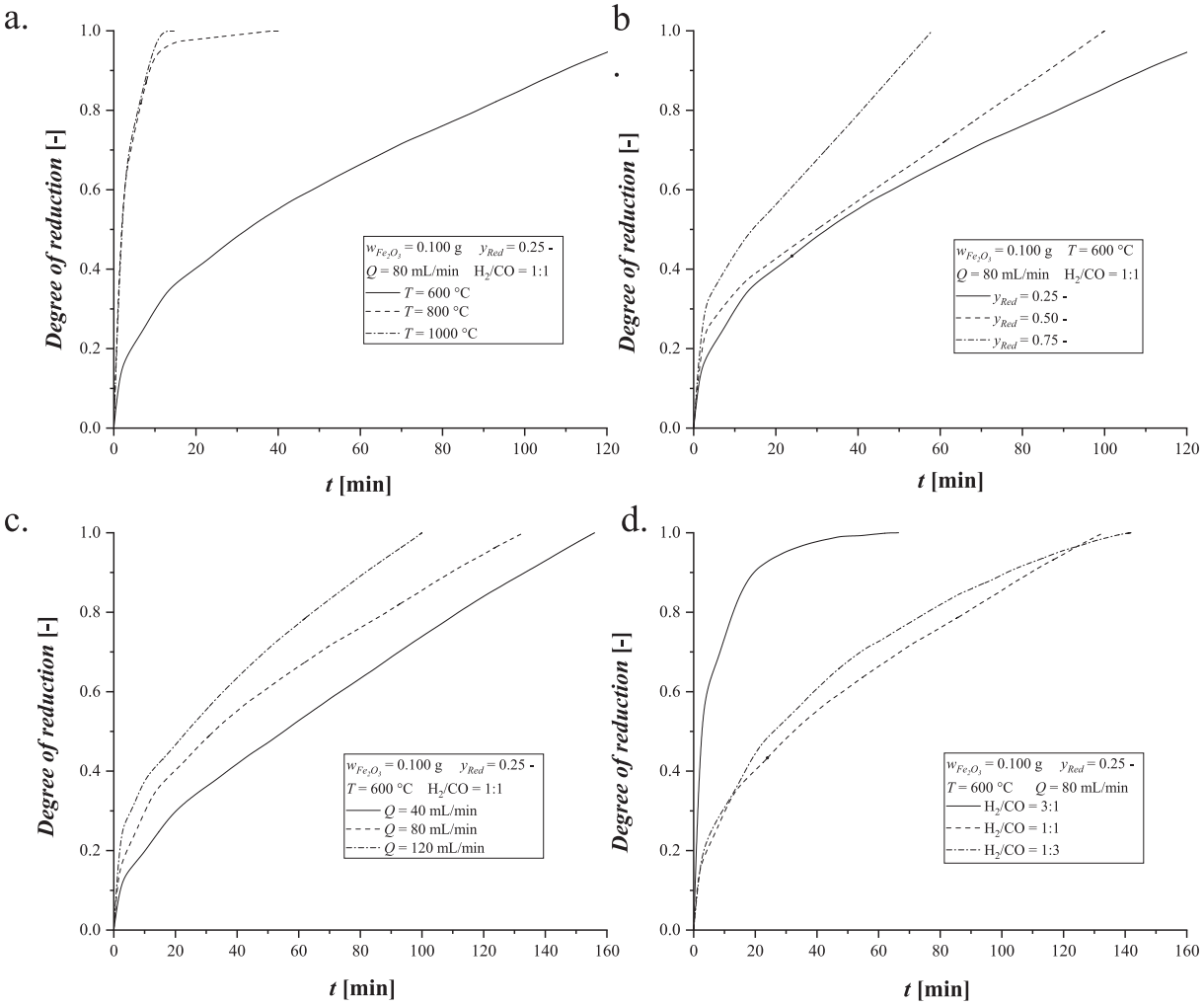

Fig. 16. Estimated reduction degree for BF pellet powder varying a) temperature, b) gas flow rate, c) molar ratio of reductants in the feed gas, and d) molar ratio between hydrogen and carbon monoxide. The experimental reproducibility was evaluated from three independent experiments. The corresponding 95% confidence intervals are smaller than the graphical resolution of the figure (relative uncertainty <5%); therefore, error bars are omitted for clarity.

reaction kinetics. Such data can support the refinement and validation of kinetic models intended for subsequent application to pellet-scale and reactor-scale simulations [37].

4. Conclusions

Reduction experiments of powders of pure hematite and ironmaking pellets in hydrogen and carbon monoxide atmosphere have been performed with the goal to gain understanding about how the different materials are reduced under different conditions. A laboratory rig was applied where small samples of powder were reduced by a gas at different composition, temperature and flow rate. By analyzing the composition of the outgoing gas, balance equations for the elements were stated. The interpretation of the experimental results was supported by morphological and chemical physical characterization with the aim of explicating the contribution of the complex reaction patterns and the phenomena associated. Based on the observed amount of carbon deposited on the samples, a model of the reduction degree of the sample was developed. The reduction of pure hematite was found to be comparatively fast, and a higher temperature further increased the reduction rate. Likewise, as expected, higher molar ratios of the reductants increased the reduction rates. Because of limited gas flow rates in the device, an increased gas flow rate also enhanced the reduction since the gas suffered from starvation of the reductants at low flow rates. At lower temperatures, carbon was deposited on the sample, but the carbon deposition was only significant at higher ratios of CO in the feed gas. Increasing the H_2:CO ratio in the feed gas was also beneficial for the reduction. Even though the overall trends observed for pure hematite were reproduced by powder of BF and DR pellets, remarkable differences were also noted. Overall, the results for BF pellet power differed most from those of pure hematite, while the DR pellet powders showed intermediate behavior. This is expected due to the low share of gangue in the DR pellets. The DR pellet powder was reduced clearly more slowly than pure hematite but faster than BF pellet powder. The carbon deposition on the commercial ironmaking materials was more severe, where the close and sintered surface morphology enhanced carbon deposition on the grains. A detailed investigation of the role of the reverse Boudouard reaction was performed through CHNS analysis. Moreover, the reduction of the BF and DR pellet powders showed more complex behavior that reflects the chemical, physical and morphological differences. The changes in the morphology also resulted in maxima and minima in the reduction rates, which could be partly explained by SEM images taken at different reaction times. The images indicate the appearance of vacancies on the surface that correspond to higher reductant consumption, and small bright and dark grains that correspond to metallic iron and graphitic carbon on a metallic carbide layer. Finally, a novel way of estimating the reduction degree was proposed and applied based on elemental balances for the gas phase combined

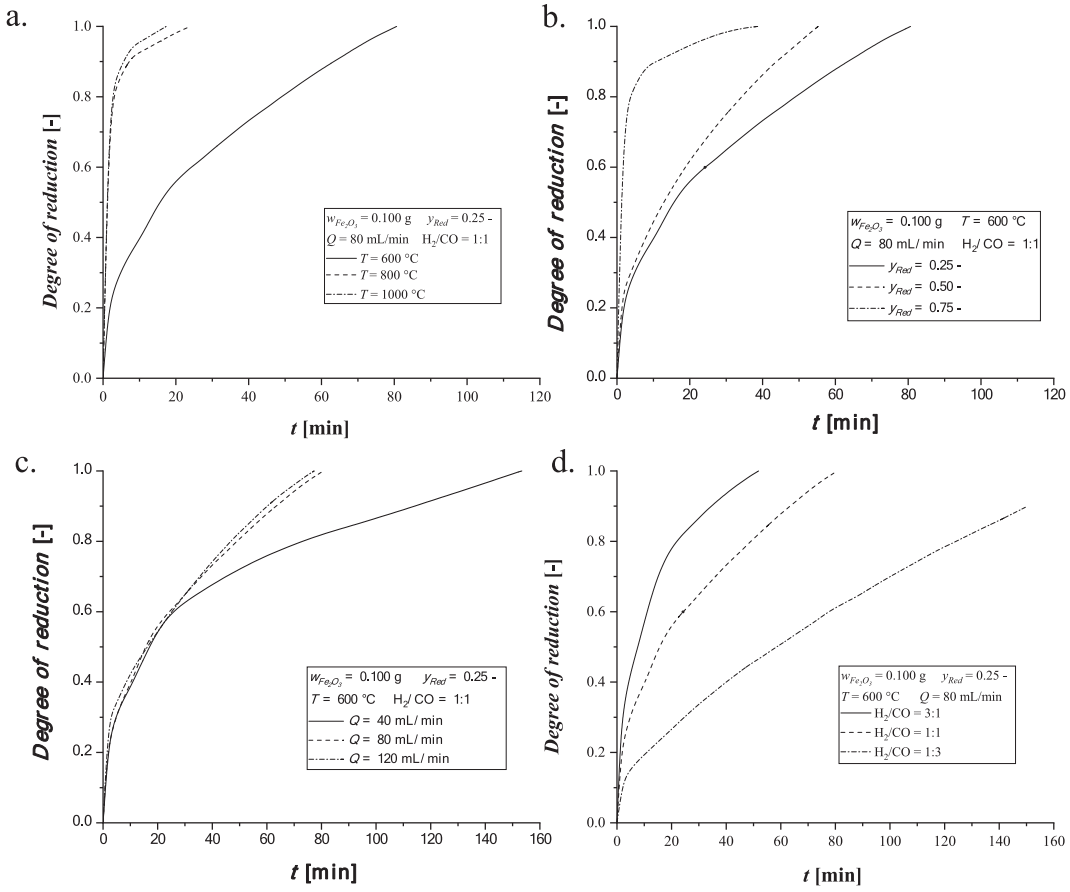

Fig. 17. Estimated reduction degree for DR pellet powder varying a) temperature, b) gas flow rate, c) molar ratio of reductants in the feed gas, and d) molar ratio between hydrogen and carbon monoxide. Experimental reproducibility was evaluated by three independent experiments. The corresponding 95% confidence intervals are smaller than the graphical resolution of the figure (relative uncertainty <5%), so error bars are omitted for clarity.

with information about the initial amount of (reduceable) oxygen in the samples as well as about the carbon deposition rate. This model was applied to study the effect of different experimental conditions on the evolution of the reduction degree of the samples. The present work on iron oxide reduction using H_2–CO gas mixtures provide important insights about the effects of reduction kinetics and the evolution of morphological characteristics of the reduced iron phase. The kinetic data obtained in this study constitutes a database for future process optimization. The operation at higher temperatures favors faster reduction kinetics and suppresses carbon deposition, thereby expanding the feasible operating window for H_2–CO mixtures. By integrating the experimentally determined reduction rates and carbon deposition behavior with process models, the optimal H_2/CO ratio can be identified as a function of hydrogen price, syngas availability, carbon taxation, and targeted CO_2 emissions. Such an integrated framework represents the next step toward designing flexible hydrogen-based direct reduction processes. Based on the detailed findings obtained in this study, several future research directions can be proposed to deepen the understanding of gas–solid interaction developing a comprehensive mechanistic model that integrate the reduction kinetics coupled with morphological changes simultaneously. Consequently, the results should not be interpreted as directly representative of the behavior of industrial pellets, where larger characteristic dimensions, pore connectivity, and coupled heat and mass transport phenomena significantly influence the overall reduction kinetics. Future research should focus on extending the present methodology to pelletized materials with controlled porosity and gangue compositions in order to evaluate the interaction between intrinsic reaction kinetics and transport limitations under realistic direct reduction conditions.

CRediT authorship contribution statement

Antonio D'Angelo: Writing – original draft, Validation, Methodology, Investigation, Formal analysis. **Emiliano Salucci:** Validation, Data curation. **Vincenzo Russo:** Writing – review & editing, Supervision. **Martino Di Serio:** Writing – review & editing, Supervision. **Henrik Grénman:** Writing – review & editing, Supervision, Project administration, Conceptualization. **Henrik Saxén:** Writing – review & editing, Supervision, Project administration, Conceptualization.

Declaration of competing interest

The authors declare that they have no known competing financial interests or personal relationships that could have appeared to influence the work reported in this paper.

Acknowledgements

We gratefully acknowledge financial support from the European Union within the projects *Minimisation of CO_2 emissions from the BF by hydrogen containing injectants and use of DRI/HBI during transition to new ironmaking processes until 2030* (grant agreement 101057790) and *Maximise H_2 Enrichment in Direct Reduction Shaft Furnaces* (grant agreement 101058429). Views and opinions expressed in the paper are, however, those of the authors only and do not necessarily reflect those of the European Union, so the European Union cannot be held responsible for them. The authors are also grateful to Dr. Antonella Giarra (Department of Chemical Science, University of Naples Federico II) for her support in the SEM characterization. Mr. Luigi Ebarone and Mr.

Francesco Levi are acknowledged for the support given to conduct the experiments included in the present article.

Appendix A

A simplified model of the system during the phases when carbon deposition occurs was created based on the elemental balances for carbon, oxygen, hydrogen and helium

$$\dot{n}_{CO}^{in} = \dot{n}_{CO_2}^{out} + \dot{n}_{CO}^{out} + \dot{n}_{C}^{dep} \tag{A1}$$

$$\dot{n}_{CO}^{in} + \dot{n}_{O}^{red} = \dot{n}_{CO}^{out} + 2\dot{n}_{CO_2}^{out} + \dot{n}_{H_2O}^{out} \tag{A2}$$

$$2\dot{n}_{H_2}^{in} = 2\dot{n}_{H_2}^{out} + 2\dot{n}_{H_2O}^{out} \tag{A3}$$

$$\dot{n}_{He}^{in} = \dot{n}_{He}^{out} \tag{A4}$$

where $\dot{n}_{O}^{red}$ is the reduction rate and $\dot{n}_{C}^{dep}$ is the carbon deposition rate. Solving the molar outflow rate of carbon monoxide from Eq. (A1) gives

$$\dot{n}_{CO}^{out} = \dot{n}_{CO}^{in} - \dot{n}_{CO_2}^{out} - \dot{n}_{C}^{dep} \tag{A5}$$

and inserting this into Eq. (A2) yields

$$\dot{n}_{CO_2}^{out} = \dot{n}_{O}^{red} + \dot{n}_{C}^{dep} - \dot{n}_{H_2O}^{out} \tag{A6}$$

Inserting this into Eq. (A5) gives, after some rearrangement,

$$\dot{n}_{CO}^{out} = \dot{n}_{CO}^{in} - \dot{n}_{O}^{red} - 2\dot{n}_{C}^{dep} + \dot{n}_{H_2O}^{out} \tag{A7}$$

From the hydrogen balance Eq. (A4) we have

$$\dot{n}_{H_2}^{out} = \dot{n}_{H_2}^{in} - \dot{n}_{H_2O}^{out} \tag{A8}$$

The water content of the outgoing gas could not be determined accurately in the experimental system, so an attempt was made to estimate this unknown variable. Since the water gas shift reaction is catalyzed by iron oxides (primarily by magnetite but also by wustite), it was assumed that the reaction is fast enough to be in equilibrium. We now have

$$K_{WGS} = \frac{y_{CO_2}^{out} \bullet y_{H_2}^{out}}{y_{CO}^{out} \bullet y_{H_2O}^{out}} = \frac{\dot{n}_{CO_2}^{out} \bullet \dot{n}_{H_2}^{out}}{\dot{n}_{CO}^{out} \bullet \dot{n}_{H_2O}^{out}} \tag{A9}$$

where y_i^{out} is the molar ratio of component i in outgoing gas.

Inserting the expressions for the molar flowrates of CO, CO_2 and H_2 from Eqs. (A6-A8), we have

$$K_{WGS} = \frac{\left(\dot{n}_{O}^{red} + \dot{n}_{C}^{dep} - \dot{n}_{H_2O}^{out}\right) \bullet \left(\dot{n}_{H_2}^{in} - \dot{n}_{H_2O}^{out}\right)}{\left(\dot{n}_{CO}^{in} - \dot{n}_{O}^{red} - 2\dot{n}_{C}^{dep} + \dot{n}_{H_2O}^{out}\right) \bullet \dot{n}_{H_2O}^{out}} \tag{A10}$$

This equation can be rearranged as

$$(1 - K_{WGS})\left(\dot{n}_{H_2O}^{out}\right)^2 + \left(K_{WGS}\left(\dot{n}_{O}^{red} + 2\dot{n}_{C}^{dep} - \dot{n}_{CO}^{in}\right) - \left(\dot{n}_{O}^{red} + \dot{n}_{C}^{dep} + \dot{n}_{H_2}^{in}\right)\right)\dot{n}_{H_2O}^{out} + \left(\dot{n}_{O}^{red} + \dot{n}_{C}^{dep}\right)\dot{n}_{H_2}^{in} = 0 \tag{A11}$$

i.e., as a second order equation in $\dot{n}_{H_2O}^{out}$. Solving this (after disregarding the negative root), the result can be inserted into Eq. (A5) to solve for $\dot{n}_{CO_2}^{out}$, into Eq. (A6) to solve for $\dot{n}_{CO}^{out}$ and finally into Eq. (A7) to solve for $\dot{n}_{H_2}^{out}$. Thus, all outgoing molar flow rates of gas are known, and the molar ratios can be determined.

To illustrate the performance of the model, it was applied to simulate the evolution of outgoing the gas composition for two cases, corresponding to the less or more severe carbon deposition encountered in the reduction of pure hematite and BF pellet fines at 873 K and with equal shares (12.5%) of hydrogen and carbon monoxide in the feed gas. The simulation was started at $t = 20$ min, which was the first time carbon deposition was noted on the samples, and when the hematite was fully reduced to magnetite. The reduction rate was determined from the gas measurements and gas balance equations while carbon deposition rate $\dot{n}_{C}^{dep}(t)$ was approximated by the Langmuir equation fitted to points where the carbon deposition was determined. Fig. A1 illustrates the measured (red crosses) and simulated (black solid line) molar ratio of carbon monoxide in the outgoing gases, as well as the molar ratio in the fed gas (dash-dotted blue line). The simulated behavior is seen to agree well with the measured mola ratio of CO in the outgoing gas, justifying the approach.

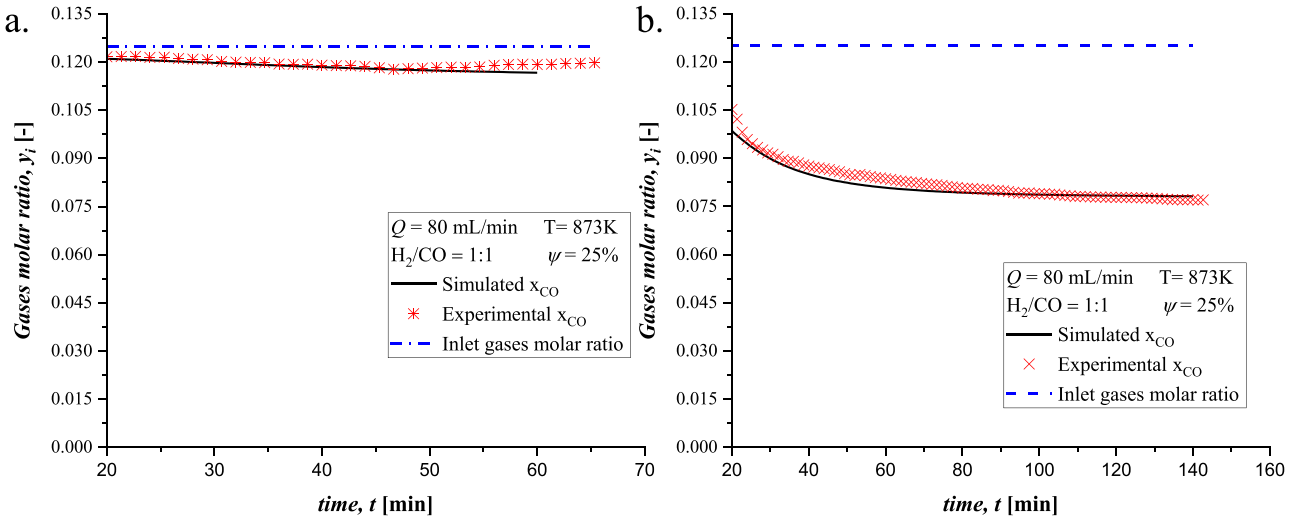

Fig. A1. Measured (red crosses) and simulated (black solid line) molar ratio of carbon monoxide in the outgoing gases as well as the molar ratio in the feed gas (dash-dotted horizontal blue line) for a) pure hematite, and b) BF pellet powders.

Appendix B. Supplementary data

Supplementary data to this article can be found online at https://doi.org/10.1016/j.cej.2026.180810.

Data availability

The authors do not have permission to share data.

References

[1] E. Salucci, A. D'Angelo, V. Russo, H. Grénman, H. Saxén, Modelling of iron oxide reduction with hydrogen in a small fixed bed, Chem. Eng. Sci. 292 (2024) 119934, https://doi.org/10.1016/j.ces.2024.119934.

[2] A. Chatterjee, Beyond the Blast Furnace, CRC Press, 1994.

[3] P. Cavaliere, A. Perrone, D. Marsano, V. Primavera, Hydrogen-based direct reduction of iron oxides pellets modeling, Steel Res. Int. 94 (2023) 2200791, https://doi.org/10.1002/srin.202200791.

[4] F. Chen, Y. Mohassab, T. Jiang, H.Y. Sohn, Hydrogen reduction kinetics of hematite concentrate particles relevant to a novel flash ironmaking process, Metall. Mater. Trans. B 46 (3) (2015) 1133–1145, https://doi.org/10.1007/s11663-015-0332-z.

[5] Factsage. Factsage Software and Databases [software], https://factsage.csom/.

[6] Y.K. Rao, A. Adjorlolo, J.H. Haberman, On the mechanism of catalysis of the Boudouard reaction by alkali-metal compounds, Carbon 20 (3) (1982) 207–212, https://doi.org/10.1016/0008-6223(82)90022-7.

[7] P.L. Walker Jr., J.F. Rakszawski, G.R. Imperial, Carbon formation from carbon monoxide-hydrogen mixtures over iron catalysts. II: rates of carbon formation, J. Phys. Chem. 62 (2) (1959) 140–149, https://doi.org/10.1021/j150572a003.

[8] H. Park, V. Sahajwalla, Effect of alumina and silica on the reaction kinetics of carbon composite pellets at 1473 K, ISIJ Int. 54 (1) (2014) 49–55, https://doi.org/10.2355/isijinternational.54.49.

[9] E. Salucci, A. D'Angelo, V. Russo, H. Grénman, H. Saxén, Review on the reduction kinetics of iron oxides with hydrogen-rich gas: experimental investigation and modeling approaches, Ind. Eng. Chem. Res. 64 (2024) 1–35, https://doi.org/10.1021/acs.iecr.4c03136.

[10] X. Mao, P. Garg, X. Hu, Y. Li, S. Nag, S. Kundu, J. Zhang, Kinetic analysis of iron ore powder reaction with hydrogen—carbon monoxide, Int. J. Miner. Metall. Mater. 29 (2022) 1882–1890, https://doi.org/10.1007/s12613-022-2512-6.

[11] K. Rechberger, A. Spanlang, A. Sasiain Conde, H. Wolfmeir, C. Harris, Green hydrogen-based direct reduction for low-carbon steelmaking, Steel Res. Int. 91 (2020) 1611–3683, https://doi.org/10.1002/srin.202000110.

[12] D. Spreitzer, J. Schenk, Reduction of iron oxides with hydrogen—a review, Steel Res. Int. 90 (2019) 1900108, https://doi.org/10.1002/srin.201900108.

[13] M.S. Valipour, Mathematical modeling of a non-catalytic gas-solid reaction: hematite pellet reduction with syngas, Sci. Iran. Trans. C: Chem. Chem. Eng. 16 (2009) 108–124. https://www.researchgate.net/publication/265078768.

[14] W. Du, S. Yang, F. Pan, J. Shangguan, J. Lu, S. Liu, H. Fan, Hydrogen reduction of hematite ore fines to magnetite ore fines at low temperatures, J. Chem. (2017) 2090–9063, https://doi.org/10.1155/2017/1919720.

[15] S. Hallström, L. Höglund, J. Ågren, Modeling of iron diffusion in the iron oxides magnetite and hematite with variable stoichiometry, Acta Mater. 59 (1) (2011) 53–60, https://doi.org/10.1016/j.actamat.2010.08.032.

[16] A. Heidari, N. Niknahad, M. Iljana, T. Fabritius, A review on the kinetics of iron ore reduction by hydrogen, Materials (Basel, Switzerland) 14 (2021) 7540, https://doi.org/10.3390/ma14247540.

[17] H. Zuo, C. Wang, J. Dong, Reduction kinetics of iron oxide pellets with H_2 and CO mixtures, Int. J. Miner. Metall. Mater. 22 (2015) 688–696, https://doi.org/10.1007/s12613-015-1123-x.

[18] W. Liu, J.Y. Lim, M.A. Saucedo, A.N. Hayhurst, S.A. Scott, J.S. Dennis, Kinetics of the reduction of wüstite by hydrogen and carbon monoxide for the chemical looping production of hydrogen, Chem. Eng. Sci. 120 (2014) 149–166, https://doi.org/10.1016/j.ces.2014.08.010.

[19] J. Oh, D. Noh, The reduction kinetics of hematite particles in H_2 and CO atmospheres, Fuel 196 (2017) 144–153, https://doi.org/10.1016/j.fuel.2016.10.125.

[20] M.L. Ali, Q. Fradet, U. Riedel, Kinetic mechanism development for the direct reduction of single hematite pellets in H_2/CO atmospheres, Steel Res. Int. 93 (2022) 2200043, https://doi.org/10.1002/srin.202200043.

[21] R. Bourab, S. Bennici, C. Mirodatos, A. Auroux, Reduction kinetics of mechanically activated hematite concentrate with hydrogen gas using non isothermal methods, J. Catal. 2014 (1) (2014) 612575, https://doi.org/10.1155/2014/612575.

[22] B. Sadeghi, P. Cavaliere, M. Bayat, N. Ebrahimzadeh Esfahani, A. Laska, D. Koszelow, Experimental study and numerical simulation on porosity dependent direct reducibility of high-grade iron oxide pellets in hydrogen, Int. J. Hydrog. Energy 69 (2024) 586–607, https://doi.org/10.1016/j.ijhydene.2024.05.050.

[23] A. Perrone, P. Cavaliere, B. Sadeghi, L. Dijon, A. Laska, D. Koszelow, Effect of TiO2 percentage on the hydrogen-based direct reducibility of high-grade pellets, carburization behavior of high-grade pellets after direct reduction in pure hydrogen, J. Sustainable Metall. 10 (2024) 1991–2008, https://doi.org/10.1007/s40831-024-00906-2.

[24] A. D'Angelo, E. Salucci, V. Russo, H. Grénman, H. Saxén, Hydrogen reduction of iron oxide powder in thin layers, Ind. Eng. Chem. Res. 64 (2025) 158–170. https://pubs.acs.org/doi/full/10.1021/acs.iecr.4c03138.

[25] A. D'Angelo, E. Salucci, V. Russo, H. Grénman, H. Saxén, Reduction kinetics of pure and industrial hematite samples with hydrogen in a small fixed bed system, Chem. Eng. J. 519 (2025) 165117, https://doi.org/10.1016/j.cej.2025.165117.

[26] D. Wagner, O. Devisme, F. Patisson, D. Ablitzer, A laboratory study of the reduction of iron oxides by hydrogen, ISIJ Int. 48 (9) (2008) 1168–1178. https://hal.science/hal-00265636v1.

[27] P. Cavaliere, B. Sadeghi, L. Dijon, A. Laska, D. Koszelow, Three-dimensional characterization of porosity in iron ore pellets: a comprehensive study, Miner. Eng. 213 (2024) 108746, https://doi.org/10.1016/j.mineng.2024.108746.

[28] B. Sadeghi, P. Cavaliere, N. Ramos Goncalves, M. Bayat, M. Aminaei, A. Laska, D. Koszelow, Reducibility of high-grade pellets directly reduced in hydrogen atmosphere: modeling and experimental procedure, Int. J. Hydrog. Energy 144 (2025) 69–84, https://doi.org/10.1016/j.ijhydene.2025.06.020.

[29] I.J. Moon, C.H. Rhee, D.J. Min, Reduction of hematite compacts by H_2–CO gas mixtures, Steel Res. 69 (8) (1998) 302–306, https://doi.org/10.1002/srin.199805555.

[30] X. Mao, B. Zhou, H. Deng, Q. Zeng, J. Li, J. Chen, Y. Xiao, K. Chou, The effect of H_2O and CO_2 on the adsorption behavior of H_2 and CO on hematite, Materials 18 (17) (2025) 4175, https://doi.org/10.3390/ma18174175.

[31] X.G. Wang, W. Weiss, S.K. Shaikhutdinov, M. Ritter, M. Petersen, F. Wagner, R. Schlögl, M. Scheffler, The hematite (α-Fe_2O_3)(0001) surface: evidence for domains of distinct chemistry, Phys. Rev. Lett. 81 (5) (1998) 1038–1041.
[32] I.R. Souza Filho, H. Springer, Y. Ma, A. Mahajan, C.C. da Silva, M. Kulse, D. Raabe, Green steel at its crossroads: hybrid hydrogen-based reduction of iron ores, Annu. Rev. Mater. Res. 52 (2022) 383–414, https://doi.org/10.48550/arXiv.2201.13356.
[33] A. Bonalde, A. Henriquez, M. Manrique, Kinetic analysis of the iron oxide reduction using hydrogen–carbon monoxide mixtures as reducing agent, ISIJ Int. 45 (9) (2005) 1255–1260, https://doi.org/10.2355/isijinternational.45.1255.
[34] K. Mondal, H. Lorethova, E. Hippo, T. Wiltowski, S.B. Lalvani, Reduction of Iron oxide in carbon monoxide atmosphere—reaction controlled kinetics, Fuel Process. Technol. 86 (2004) 33–47, https://doi.org/10.1016/j.fuproc.2003.12.009.
[35] F. Lu, L. Wen, Y. Chen, H. Zhong, J. Xu, S. Zhang, Z. Yang, Carbon formation on the surface during the reduction of iron oxide particles by CO and CO/H_2 mixtures, Chem. Eng. Sci. 205 (2019) 238–247.
[36] The International Centre for Diffraction Data [dataset]. https://www.icdd.com/pdf-5/.
[37] A.M. Soodmand, A. Heidari, S. K., M. Azadi, A. Iljana, M.K. Heikkilä, S. Ghosalva, P. Urpelainen, L. Cavaliere, V. Dijon, T. Morais, Fabritius, Effect of water vapor on the reduction and carburization of Iron ore pellets: theoretical and experimental approaches, Metall. Mater. Trans. B 56 (2025) 4552–4570, https://doi.org/10.1007/s11663-025-03745-y.
[38] Q. Meng, J. Lin, R. Weng, H. Long, T. Chun, P. Wang, Z. Di, L. Dessbesell, C. Xu, Effects of gangue compositions on reduction process of carbon-bearing iron ore pellets, J. Iron Steel Res. Int. 25 (2018) 1105–1112, https://doi.org/10.1007/s42243-018-0168-2.